Using the Voids. Evidence for an Antenna Effect in Dye-Sensitized Mesoporous TiO_2 Thin Films†

Paul G. Hoertz,‡ Anna Goldstein, Carrie Donley,§ and Thomas J. Meyer*

Department of Chemistry, University of North Carolina at Chapel Hill, Chapel Hill, North Carolina 27599-3290

Received: April 28, 2010; Revised Manuscript Received: June 27, 2010

Composite structures of $Ru(bpy)_2(4,4'\text{-}(PO_3H_2)_2bpy)^{2+}$ surface bound to nanocrystalline TiO_2 with an overlayer of $Ru(bpy)_3^{2+}$ ion exchanged into Nafion, FTO|nanoTiO_2-$[Ru(bpy)_2(4,4'\text{-}(PO_3H_2)_2bpy)]^{2+}$/Nafion,$Ru(bpy)_3^{2+}$ (FTO = fluorine-doped tin oxide), have been prepared and characterized. Steady-state emission and time-resolved lifetime measurements demonstrate that energy transfer occurs from Nafion,$Ru(bpy)_3^{2+*}$ to adsorbed $Ru(bpy)_2(4,4'\text{-}(PO_3H_2)_2bpy)^{2+}$ with an efficiency of ~0.49. Energy transfer sensitizes photoinjection by the adsorbed metal-to-ligand charge transfer (MLCT) excited state by an "antenna effect."

Introduction

In dye-sensitized solar cells (DSSCs), solar to electrical conversion efficiencies of up to 10−11% have been reached with optimization.[1,2] These cells typically utilize surface adsorption of chemically bound or adsorbed molecular "dyes" in films of nanostructured, ~15−20 nm TiO_2 particles (nanoTiO_2) on a conductive substrate, which act as photoanodes.[1,2] Interparticle voids are filled with a solution electrolyte and a redox carrier, typically I_3^-/I^-, or a conducting polymer.[1,2] In solution cells, excitation and injection by the excited state of the dye is followed by I^- oxidation to I_3^- and diffusion through the voids to an external cathode. An issue is film thickness, *d*, and minimization of the transfer distance required for photoinjected electrons to reach the underlying collector electrode. At constant surface area, thinner films can lead to higher efficiencies if *d* is greater than $1/\alpha$, with α being the penetration depth of light, and *d* being less than the electron diffusion length, *L*.[1]

We report here demonstration of an "antenna" effect within the interparticle voids of nanoTiO_2 films, which enhances light absorption and leads to energy transfer sensitization of surface photoinjection. Configurations of this kind could be of value in extending light absorption over a broader spectral region and in decreasing film thicknesses below *L* while maintaining high light absorptivity.

In the strategy pursued here, an antenna within the interparticle voids is created in an overlayer of the ion exchange polymer Nafion on top of the surface-bound complex $Ru(bpy)_2(4,4'\text{-}(PO_3H_2)_2bpy)^{2+}$ on TiO_2 (TiO_2−Ru^{II}) (Figure 1). A second, cationic chromophore was added to the Nafion overlayer by ion exchange. The phosphonate derivatived complex was used for initial surface attachment rather than a carboxylate derivative because of the aqueous stability of phosphonate-surface links toward hydrolysis and loss in aqueous solutions, which enables loading of Nafion in aqueous solutions. Stabilized phosphonate surface binding and aqueous stability are also key in solar fuel reactions such as water splitting and CO_2 reduction.[3]

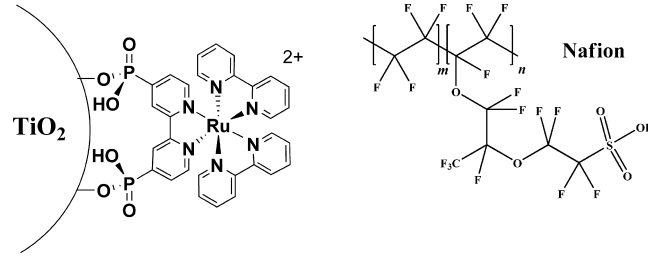

Figure 1. Structures of surface-bound $Ru(bpy)_2(4,4'\text{-}(PO_3H_2)_2bpy)^{2+}$ (TiO_2−Ru^{II}) and Nafion.

Experimental Section

Materials. Nafion perfluorinated resin solution (5 wt %) in a mixture of lower aliphatic alcohols and water (Aldrich, 45% water, equivalent weight = 1100), acetonitrile (Fisher), methanol (Fisher), ethanol, perchloric acid, lithium iodide (Aldrich), and iodine were all used as received. The complexes and complex salts $[Ru(bpy)_2(4,4'\text{-}(PO_3H_2)_2bpy)](PF_6)_2$ and $[Ru(bpy)_3](Cl)_2$ were prepared and characterized according to literature procedures.[4,5] Nanocrystalline TiO_2 films (nanoTiO_2) were prepared by a previously published procedure.[6]

Nafion Films on Fluorine-Doped Tin Oxide (FTO): FTO|Nafion. A pool of Nafion perfluorinated resin solution was deposited on freshly sonicated/cleaned FTO slides (5 cm ×1.1 cm). The substrate was tilted at a ~45° angle until drops of Nafion no longer fell from the substrate, was briefly held vertically, and the bottom side was blotted with a Kimwipe to remove excess Nafion solution and placed on a flat surface to air-dry slowly. The area of the Nafion thin films was controlled by masking with Kapton tape, which was removed when the film was dry. Typical film thicknesses were ~0.8−1 μm as determined by profilometry. Metal complex cations were subsequently added to the Nafion by placing dry films in neutral aqueous solutions containing the cation (1 mM) for several hours to days.

Surface Loading on nanoTiO_2. The phosphonate derivatized complex was bound to FTO|nanoTiO_2 by placing FTO|nanoTiO_2

† Part of the "Michael R. Wasielewski Festschrift".

* Corresponding author. E-mail: tjmeyer@unc.edu.

‡ Current address: RTI International, Center for Aerosol Technology, Research Triangle Park, NC 27709.

§ Also affiliated with the Institute of Advanced Materials Nanoscience and Technology, University of North Carolina at Chapel Hill, Chapel Hill, NC 27599-3290.

10.1021/jp103867j
Published on Web 08/16/2010

films in 0.1 mM methanol solutions of $[Ru(bpy)_2(4,4'\text{-}(PO_3H_2)_2bpy)](PF_6)_2$ for at least 12 h. The loaded film was rinsed with methanol and air-dried.

Nafion Overlayer. FTO|nanoTiO_2 (FTO|TiO_2) or FTO|nano-TiO_2−$Ru(bpy)_2(4,4'\text{-}(PO_3H_2)_2bpy)^{2+}$ (TiO_2−Ru^{II}) slides were immersed in Nafion perfluorinated resin solution (5 wt %) for 2−48 h (typically 15 or 48 h); the Nafion solutions were 0.1 M in $HClO_4$.[3] The slides were removed and rinsed exhaustively in the following sequence: (1) deionized water, (2) 1:1 deionized water/methanol, and (3) methanol. Samples were air-dried and stored in the dark until further use.

Addition of Complex Cations. TiO_2 or FTO|TiO_2−Ru^{II} slides with a Nafion overlayer were immersed in aqueous pH = 7 solutions containing mM $[Ru(bpy)_3](Cl)_2$ for 3−15 h. The samples were rinsed with either acetonitrile or methanol and air-dried.

Measurements. UV−visible (UV−vis) spectra were recorded on an Agilent Technologies model 8453 diode-array spectrophotometer. Steady-state emission spectra were collected on a PTI QuantaMaster-4SE spectrofluorimeter with a Hamamatsu R-928 photomultiplier tube. Time-resolved emission data were collected on a PTI GL-301 dye laser, pumped by a PTI GL-3000 pulsed nitrogen laser with a McPherson 272 monochromator and a Hamamatsu R-928 photomultiplier. Film thicknesses were determined with a Tencor alpha step 200 profilometer.

For incident photon-to-current efficiency (IPCE) measurements, light output from an Oriel 75 W xenon lamp was passed through an Oriel Cornerstone 260 monochromator to produce monochromatic light from 300 to 900 nm with a bandwidth of 10 nm. Photocurrents were measured with a Keithley 6517A electrometer. Light power was monitored with a UDT S370 optometer equipped with a UDT 260 detector. Prior to experimental measurements, the samples were incubated in 0.1 M $HClO_4$ until an amount of non ion-exchanged $Ru(bpy)_3^{2+}$ was lost as shown by UV−vis measurements.

Average lifetimes were calculated by fitting decay curves to the stretched exponential Kohlrausch−Williams−Watts distribution function (eq 1) with $I(t)$ being the intensity at time t and I_o being that at $t = 0$.[7]

$$I(t) = I_o \cdot \exp[-(t/\tau_o)^{\beta}] \quad (1)$$

In eq 1, β is a measure of the width of the distribution, and τ_o is the lifetime with $\beta = 1$ for exponential behavior. The average lifetime for the distribution is given by eq 2.

$$\langle\tau\rangle = \tau_o \Gamma\left(1 + \frac{1}{\beta}\right) \quad (2)$$

The gamma function, Γ, is defined by $\Gamma(z) = \int_0^\infty x^{z-1}\, e^{-x}\, dx$.

X-ray Photoelectron Spectroscopy. X-ray photoelectron spectra (XPS) were obtained at the Chapel Hill Analytical and Nanofabrication Laboratory (CHANL) at UNC with a Kratos Analytical Axis UltraDLD spectrometer with monochromatized X-ray Al Kα radiation (1486.6 eV). Survey scans were performed with a step size of 1 eV and a pass energy of 80 eV. High-resolution scans were conducted with a step size of 0.1 eV and a pass energy of 20 eV. The high-resolution data were fit with a Gaussian−Lorentzian product function that was weighted 30% Lorentzian. The binding energies for various XPS peaks (Ru 3d, Cl 2p, S 2p) were referenced to internal C 1s peaks.

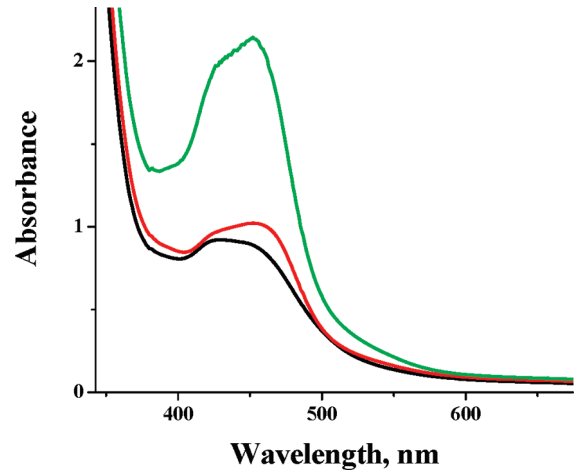

Figure 2. UV−vis spectra of FTO|nanoTiO_2−$[Ru(bpy)_2(4,4'\text{-}(PO_3H_2)_2bpy)]^{2+}$ loaded from methanol (black line), immersed in 5 wt % Nafion solution (0.1 M $HClO_4$) for 2 days with rinsing (red line), and following immersion in a millimolar aqueous solution of $[Ru(bpy)_3](Cl)_2$ for 24 h (green line).

Results

Surface Coverage and Composition. Monolayer surface coverages of $Ru(bpy)_2(4,4'\text{-}(PO_3H_2)_2bpy)^{2+}$ on FTO|nanoTiO_2 (film thickness = 6 μm) were prepared by exposing FTO|nanoTiO_2 films to methanolic solutions 0.1 mM in complex for 12−18 h. UV−vis spectral measurements were used to determine surface coverages based on $\varepsilon = 9300\ M^{-1}\ cm^{-1}$ at 453 nm for $Ru(bpy)_2(4,4'\text{-}(PO_3H_2)_2bpy)^{2+}$ in methanol.[4] Typical surface coverages were $\sim 5.0 \times 10^{-8}$ mol/cm^2 or $\sim 8.3 \times 10^{-9}$ mol/cm^2-μm. The derivatized films were subsequently soaked in solutions containing 5% by weight Nafion in methanol−water mixtures for 15−48 h to add a Nafion overlayer. The Nafion solutions were 0.1 $HClO_4$.

The resulting surface structures, FTO|nanoTiO_2−$Ru(bpy)_2(4,4'\text{-}(PO_3H_2)_2bpy)^{2+}$/Nafion, were analyzed by XPS. The S/Ru normalized peak intensity ratio was 7 after a 15 h exposure time to Nafion, pointing to surface multilayer formation. Simple anion exchange of the initial PF_6^- surface counterions would only require S/Ru = 2. Exposure to the external Nafion solution for 2 days increased the S/Ru ratio to 12; a 2 h exposure gave S/Ru = 3.6. Photophysical and IPCE measurements were conducted on films with S/Ru = 12. An XPS depth profile was attempted for films stabilized with Nafion in order to determine whether S/Ru ratios were maintained within the mesoporous film structures, but was unsuccessful with only binding energies for Ti and O observed following 3 min of Argon ion sputtering.

With multilayers and excess anionic sites, the possibility exists for electrostatic binding of added cations. Ion exchange of $Ru(bpy)_3^{2+}$ into the overlayer films was monitored by UV−vis measurements (Figure 2). Increases in absorption consistent with cation loading were apparent on the seconds time scale with limiting coverages achieved after 5−15 h. For overlayers with S/Ru = 12, surface coverages of $Ru(bpy)_3^{2+}$ approaching $\sim 8 \times 10^{-8}$ mol/cm^2 were reached for 6 μm films ($\sim 1.3 \times 10^{-8}$ mol/cm^2-μm) as calculated spectrophotometrically by using $\varepsilon = 14\ 100\ M^{-1}\ cm^{-1}$ at 451 nm in water. On the basis of the UV−vis measurements, the ratio of surface-bound to electrostatically bound (Nafion) Ru was 0.9−1.4, as determined for a series of films.

Incorporation of $Ru(bpy)_3^{2+}$ into Nafion on 6 μm underivatized FTO|nanoTiO_2 was also investigated. FTO|nanoTiO_2/Nafion films (see Experimental Section) were immersed in

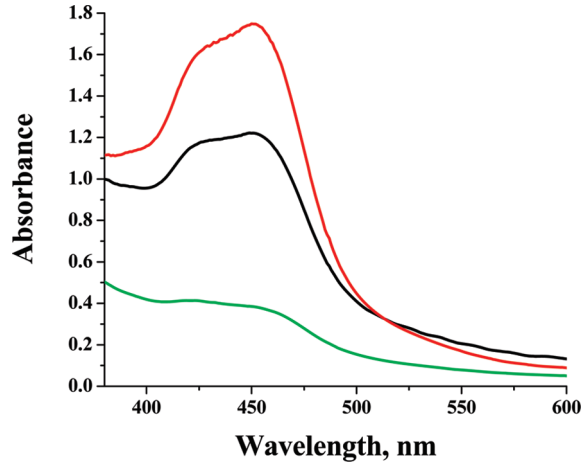

Figure 3. FTO|nanoTiO$_2$/Nafion films prepared by immersion of FTO|nanoTiO$_2$ in 5 wt% Nafion (0.1 M $HClO_4$) for 15 h (black line) or 2 days (red line) followed by exposure to a millimolar aqueous solution of $[Ru(bpy)_3](Cl)_2$ for 24 h. The green line corresponds to FTO|nanoTiO$_2$/Nafion prepared without acidification of the 5 wt% Nafion resin solution (as received from Aldrich).

aqueous solutions containing $[Ru(bpy)_3](Cl)_2$ (~1 mM) with $Ru(bpy)_3^{2+}$ incorporation monitored spectrometrically.

As shown by the spectrophotometric data in Figure 3, loading Nafion with $Ru(bpy)_3^{2+}$ from 0.1 M $HClO_4$ for 15 h gave a $Ru(bpy)_3^{2+}$ surface coverage of 7.5×10^{-8} mol/cm^2 ($\sim 1.2 \times 10^{-10}$ mol/cm^2 μm) with an increase of 1.5 for a 2 day Nafion soaking period. Loading the Nafion using the as-received resin gave a ~4-fold lower $Ru(bpy)^{2+}$ surface coverage: 1.8×10^{-8} mol/cm^2. There is a benefit in using 0.1 M $HClO_4$ to load Nafion on FTO|nanoTiO$_2$ presumably due to surface protonation of nanoTiO$_2$, which mimimizes electrostatic repulsion between nanoTiO$_2$ and polyanionic Nafion.[8]

Fill Fraction. An estimate was made of the *fill fraction*, the fraction of the mesoporous internal volume occupied by Nafion,$Ru(bpy)_3^{2+}$ in the FTO|nanoTiO$_2$−$[Ru(bpy)_2(4,4'\text{-}(PO_3H_2)_2bpy)]^{2+}$/Nafion,$Ru(bpy)_3^{2+}$ overlayer structures and in FTO|nanoTiO$_2$−Nafion/$[Ru(bpy)_3]^{2+}$ with no surface adsorbed complex. Independently, 6 μm FTO|Nafion, $Ru(bpy)_3^{2+}$ thin films were prepared to determine the maximum surface coverage of $Ru(bpy)_3^{2+}$ in pure Nafion films. The surface coverages of $Ru(bpy)_3^{2+}$ were determined spectrophotometrically giving an average value of 4.9×10^{-7} mol/cm^2. Since the average porosity of a nanoTiO$_2$ film is ~60%, the maximum possible $Ru(bpy)_3^{2+}$ surface coverage in FTO|nanoTiO$_2$−Nafion/$[Ru(bpy)_3]^{2+}$ is 2.9×10^{-7} mol/cm^2, i.e., the surface coverage of $Ru(bpy)_3^{2+}$ if all of the mesoporous void space were occupied by Nafion.[9] The surface coverages of $Ru(bpy)_3^{2+}$ for 6 μm nanoTiO$_2$ films treated with Nafion were (i) FTO |nanoTiO$_2$−$[Ru(bpy)_2(4,4'\text{-}(PO_3H_2)_2bpy)]^{2+}$/Nafion,$Ru(bpy)_3^{2+}$ = 7.8×10^{-8} mol/cm^2 and (ii) FTO|nanoTiO$_2$ -Nafion/$[Ru(bpy)_3]^{2+}$ = 7.5×10^{-8} mol/cm^2. The fill fraction is calculated by dividing these values by the maximum possible $Ru(bpy)_3^{2+}$ surface coverage. Thus, for FTO|nanoTiO$_2$−Nafion,$Ru(bpy)_3^{2+}$, the fill fraction is ~26%, while for FTO|nanoTiO$_2$−$[Ru(bpy)_2(4,4'\text{-}PO_3H_2)_2bpy)]^{2+}$/Nafion,$Ru(bpy)_3^{2+}$ the fill fraction is 27%.

The average pore diameter in the nanoTiO$_2$ films used here was shown to be ~20 nm in previous studies.[9] By treating the internal pore volume as a cube and using the above fill fractions, the thickness of the Nafion layer in the samples described above is ~3.5 nm. In the case of FTO |nanoTiO$_2$−$[Ru(bpy)_2(4,4'\text{-}(PO_3H_2)_2bpy)]^{2+}$/Nafion,$Ru(bpy)_3^{2+}$, the Nafion layer is formed on top of a ~1.5 nm thick monolayer of surface-bound sensitizer; note the physical models for FTO|nanoTiO$_2$−$[Ru(bpy)_2(4,4'\text{-}(PO_3H_2)_2bpy)]^{2+}$/Nafion,$Ru(bpy)_3^{2+}$ and FTO|nanoTiO$_2$,Nafion,$Ru(bpy)_3^{2+}$ in Figure 4.

Emission Spectra and Lifetimes. In acidic solutions at pH = 1, there is no obvious emission above background from FTO|nanoTiO$_2$−$[Ru(bpy)_2(4,4'\text{-}(PO_3H_2)_2bpy)]^{2+}$ (TiO_2−Ru^{II}) due to rapid injection, as expected.[2] As shown in Figure 5, a significant decrease in emission intensity occurs for $Ru(bpy)_3^{2+*}$ in Nafion on TiO_2 compared to FTO|Nafion,$Ru(bpy)_3^{2+*}$. A further decrease occurs for $Ru(bpy)_3^{2+*}$ in Nafion as an overlayer on surface-adsorbed $Ru(bpy)_2(4,4'\text{-}(PO_3H_2)_2bpy)^{2+}$ in FTO|nanoTiO$_2$-$[Ru(bpy)_2(4,4'\text{-}(PO_3H_2)_2bpy)]^{2+}$/Nafion,$Ru(bpy)_3^{2+}$.

Excited state decays are nonexponential in Nafion, which is typical for metal-to-ligand charge transfer (MLCT) excited-state decay in nonisotropic media given their charge transfer character and sensitivity to environmental effects.[10,11] As found in other polymeric film environments,[11,12] lifetimes were satisfactorily fit to the Kohlrausch−Williams−Watts distribution function (eq 1), with β being a measure of the breadth of the distribution. The average lifetime, $\langle\tau\rangle$, is defined in eq 2.

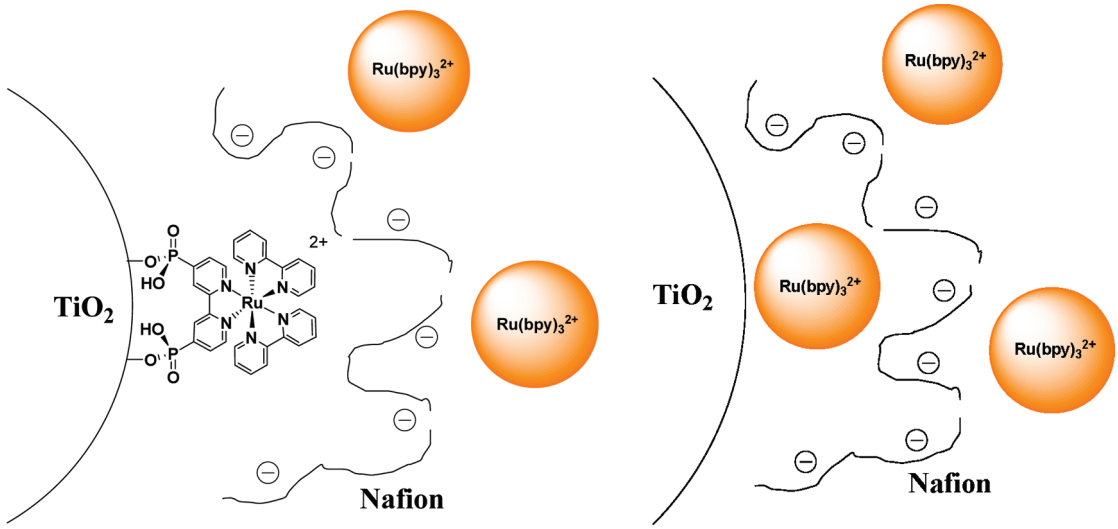

Figure 4. Schematic illustrations of $Ru(bpy)_3^{2+}$ ion exchanged into Nafion either in FTO|nanoTiO$_2$−$[Ru(bpy)_2(4,4'\text{-}(PO_3H_2)_2bpy)]^{2+}$/Nafion,$Ru(bpy)_3^{2+}$ (left) or FTO|nanoTiO$_2$−Nafion/$[Ru(bpy)_3]^{2+}$ (right).

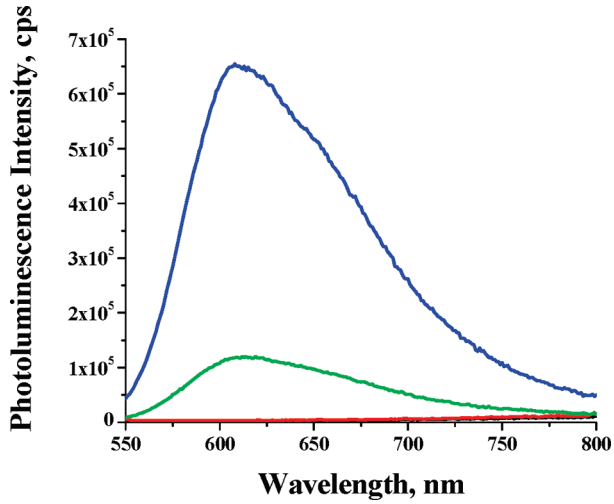

Figure 5. Steady-state emission in counts/sec with 450 nm excitation for 6 μm FTO|nanoTiO$_2$−[Ru(bpy)$_2$(4,4′-(PO$_3$H$_2$)$_2$bpy)](PF$_6$)$_2$ (8.7×10^{-8} mol/cm^2) (black line), FTO|nanoTiO$_2$−[Ru(bpy)$_2$(4,4′- (PO$_3$H$_2$)$_2$bpy)]$^{2+}$/Nafion (red line), FTO|nanoTiO$_2$−[Ru(bpy)$_2$(4,4′-(PO$_3$H$_2$)$_2$bpy)]$^{2+}$/Nafion,Ru(bpy)$_3^{2+}$ (2:1 surface bound:Ru(bpy)$_3^{2+}$) (green line), and FTO|Nafion,Ru(bpy)$_3^{2+}$ (blue line). Each slide was immersed in nitrogen-purged 0.1 M HClO$_4$ (aq). The spectra were reproducible to ±10%, and the apparent increases at longer wavelengths for the red and black spectra are an artifact.

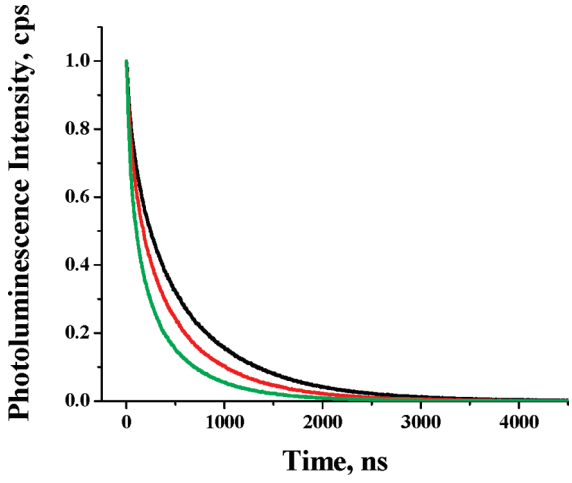

Figure 6. As in Figure 5, emission decay profiles at 610 nm following 450 nm excitation of FTO|Nafion,Ru(bpy)$_3^{2+}$ (black line, $\tau = 499 \pm 50$ ns, $k = 2.0 \times 10^6$ s^{-1}), FTO|nanoTiO$_2$−Nafion,Ru(bpy)$_3^{2+}$ (red line, $\tau = 381 \pm 40$ ns; $k = 2.6 \times 10^6$ s^{-1}), and FTO|nanoTiO$_2$−[Ru(bpy)$_2$(4,4′-(PO$_3$H$_2$)$_2$bpy)]$^{2+}$/Nafion,Ru(bpy)$_3^{2+}$ (green line, $\tau = 257 \pm 25$ ns; $k = 3.9 \times 10^6$ s^{-1}). Each slide was immersed in nitrogen-purged 0.1 M HClO$_4$.

The trends observed in the steady-state spectra are apparent in decreases in lifetimes as shown in Figure 6. Analysis of the emission−time decay profiles by eq 1 gave average lifetimes of $\langle\tau\rangle = 499 \pm 50$ ns for Ru(bpy)$_3^{2+}$* in Nafion on FTO, $\langle\tau\rangle = 381 \pm 40$ ns for Ru(bpy)$_3^{2+}$* in Nafion on TiO$_2$ (pH = 1 HClO$_4$ (aq)), and 257 ± 25 ns for Ru(bpy)$_3^{2+}$* in the Nafion overlayer in FTO|nanoTiO$_2$−[Ru(bpy)$_2$(4,4′-(PO$_3$H$_2$)$_2$bpy)]$^{2+}$/Nafion, Ru(bpy)$_3^{2+}$.

IPCE Measurements. Preliminary IPCE measurements were conducted on FTO|nanoTiO$_2$−[Ru(bpy)$_2$(4,4′-(PO$_3$H$_2$)$_2$bpy)]$^{2+}$,FTO|nanoTiO$_2$−[Ru(bpy)$_2$(4,4′-(PO$_3$H$_2$)$_2$bpy)]$^{2+}$/Nafion, FTO|nanoTiO$_2$−[Ru(bpy)$_2$(4,4′-(PO$_3$H$_2$)$_2$bpy)]$^{2+}$/Nafion,Ru(bpy)$_3^{2+}$, and FTO|nanoTiO$_2$−Nafion,Ru(bpy)$_3^{2+}$ films as photoanodes in DSSC configurations (Figure 7). The measurements were carried out at 23 ± 2 °C in 0.1 M HClO$_4$

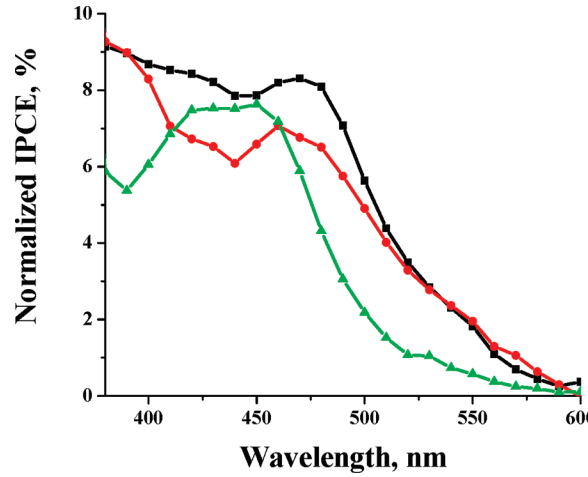

Figure 7. Normalized IPCEs for FTO|nanoTiO$_2$−[Ru(bpy)$_2$(4,4′-(PO$_3$H$_2$)$_2$bpy)]$^{2+}$/Nafion (black line with squares), FTO|nanoTiO$_2$−[Ru(bpy)$_2$(4,4′-PO$_3$H$_2$)$_2$bpy)]$^{2+}$/Nafion,Ru(bpy)$_3^{2+}$ (red line with circles), and FTO|nanoTiO$_2$−Nafion,Ru(bpy)$_3^{2+}$ (green line with triangles). The IPCE spectra were normalized relative to one another based on the APCEs at 450 nm.

with 0.6 M LiI added to reduce Ru(III) following photoinjection. With high concentrations of I_2/I_3^-, there is a complication from apparent I_3^- ion pairing to the surface bound complex.[3] Under these conditions, without added I_2 and I_3^- as the redox carrier, protons are presumably reduced to H_2 at the cathode with the net reaction observed, $2H^+ + 3I^- + 2h\nu \rightarrow H_2 + I_3^-$.

IPCE results followed the absorbance-wavelength profiles in Figure 1. For ease of comparison, IPCEs were normalized to absorbed photon-to-current efficiency (APCE) at 450 nm as defined in eq 3.

$$\text{APCE} = \frac{\text{IPCE}}{\alpha} = \varphi\eta \qquad (3)$$

In eq 3, α is the fraction of light absorbed, φ the quantum yield for injection, and η is the electron collection efficiency. With added I^- in 0.1 M HClO$_4$, APCE ∼ 20% for FTO/nanoTiO$_2$−[Ru(bpy)$_2$(4,4′-(PO$_3$H$_2$)$_2$bpy)]$^{2+}$ at the MLCT maximum at 450 nm. Addition of the Nafion overlayer decreases APCE(450 nm) to ∼8% and to ∼7% in FTO/nanoTiO$_2$−[Ru(bpy)$_2$(4,4′-(PO$_3$H$_2$)$_2$bpy)]$^{2+}$/Nafion,Ru(bpy)$_3^{2+}$. The drop in APCE with the outer Nafion layer may originate from Nafion's cation exchange character decreasing the interfacial concentration of I^- at the interface and thereby decreasing the rate of TiO$_2$−Ru^{III} reduction following photoinjection. The APCE (450 nm) for FTO|nanoTiO$_2$−Nafion/Ru(bpy)$_3^{2+}$ is also ∼8%, even in the absence of the surface-bound sensitizer.

Discussion

Intramolecular energy transfer within molecular assemblies attached to nanocrystalline TiO_2 has been treated theoretically, and intermolecular antenna effects on TiO_2 have also been explored.[13−15] Recent studies have also demonstrated Förster energy transfer between solution-phase energy donors and surface-bound energy acceptors, resulting in improved photocurrent yields.[16,17] The approach taken here involved a different strategy. Cationic light absorbers were added as an overlayer to a surface-bound Rubpy chromophore by ion exchange into the cation exchange membrane Nafion.

Film Structure. In the films used for photophysical measurements on FTO|nanoTiO$_2$−[Ru(bpy)$_2$(4,4′-(PO$_3$H$_2$)$_2$bpy)]$^{2+}$/Nafion, XPS measurements reveal a S/Ru ratio of 12:1. In these films, two of the ∼12 $-SO_3^-$ groups are utilized for charge neutralization with surface-bound [Ru(bpy)$_2$(4,4′-(PO$_3$H$_2$)$_2$bpy)]$^{2+}$. In 6 μm FTO|nanoTiO$_2$−[Ru(bpy)$_2$(4,4′-(PO$_3$H$_2$)$_2$bpy)]$^{2+}$/Nafion,Ru(bpy)$_3^{2+}$ films, loading of Ru(bpy)$_3^{2+}$ in Nafion gave ∼8 × 10^{-8} mol/cm^2, and the surface coverage of [Ru(bpy)$_2$(4,4′-(PO$_3$H$_2$)$_2$bpy)]$^{2+}$ was ∼9 × 10^{-8} mol/cm^2. In films with and without surface-bound sensitizer, Ru(bpy)$_3^{2+}$ is presumably distributed homogeneously throughout the Nafion overlayers.

On the basis of XPS and UV−vis results, the Nafion layer in FTO|nanoTiO$_2$−[Ru(bpy)$_2$(4,4′-(PO$_3$H$_2$)$_2$bpy)]$^{2+}$/Nafion, Ru(bpy)$_3^{2+}$ occupies ∼27% of the total pore volume. Since the average pore diameter is ∼20 nm,[9] the Nafion layer is ∼3.5 nm thick on the outside of the pores and the inner, surface-bound FTO|nanoTiO$_2$−[Ru(bpy)$_2$(4,4′-(PO$_3$H$_2$)$_2$bpy)]$^{2+}$ layer is ∼1.5 nm.

Photophysics. Evidence for an Antenna Effect. Emission and lifetime data in Figures 5 and 6 provide clear evidence for excited-state quenching of Ru(bpy)$_3^{2+}$* in Nafion either as a film directly on TiO$_2$ (eq 4) or, to an even greater extent, in an overlayer on TiO$_2$−Ru^{II}. The decrease in average lifetime in Nafion on TiO$_2$ is 24%, and in the Nafion overlayer it is 48% compared to FTO or glass as the underlying substrate.

$$\mathrm{TiO_2|Nafion,\ Ru(bpy)_3^{2+} \rightarrow TiO_2|Nafion,Ru(bpy)_3^{2+*} \rightarrow TiO_2(e^-)|Nafion,Ru(bpy)_3^{3+}} \quad (4)$$

A kinetic model for excited-state quenching in FTO|nanoTiO$_2$−[Ru(bpy)$_2$(4,4′-(PO$_3$H$_2$)$_2$bpy)]$^{2+}$/Nafion,Ru(bpy)$_3^{2+}$ (TiO$_2$−Ru^{II},Ru(bpy)$_3^{2+}$*(naf)) is shown in eqs 5a and 5b. In this scheme, the average lifetime of Ru(bpy)$_3^{2+}$* in Nafion in the absence of quenching is $\langle\tau_o\rangle = \langle k_o\rangle^{-1} = 499 \pm 50$ ns, $\langle k_{mig}\rangle$ is the average rate constant for energy transfer migration among Ru(bpy)$_3^{2+}$ sites in Nafion, and $\langle k_{en}\rangle$ is the rate constant for energy transfer from Ru(bpy)$_3^{2+*}$ in Nafion to surface-bound Ru(bpy)$_2$(4,4′-(PO$_3$H$_2$)$_2$bpy)$^{2+}$ (TiO$_2$−Ru^{II}). The rate constant for quenching by injection is k_q′.

$$\mathrm{TiO_2{-}Ru^{II},Ru(bpy)_3^{2+}(naf)} \xrightarrow{h\nu} \mathrm{TiO_2{-}Ru^{II*},Ru(bpy)_3^{2+}(naf)} \xrightarrow{k_q'} \mathrm{TiO_2(e^-){-}Ru^{III},Ru(bpy)_3^{2+}(naf)} \quad (5a)$$

$$\mathrm{TiO_2{-}Ru^{II},Ru(bpy)_3^{2+},Ru(bpy)_3^{2+}(naf)} \xrightarrow{h\nu} \mathrm{TiO_2{-}Ru^{II},Ru(bpy)_3^{2+},Ru(bpy)_3^{2+*}(naf)} \xrightarrow{k_{en},\ k_{mig}} \mathrm{TiO_2{-}Ru^{II*},Ru(bpy)_3^{2+}(naf)} \xrightarrow{k_q'} \mathrm{TiO_2(e^-){-}Ru^{III},Ru(bpy)_3^{2+}(naf)} \quad (5b)$$

$$k_q', k_{en} >> k_{mig}$$

On the basis of emission energies for Ru(bpy)$_3^{2+}$* in Nafion (610 nm, 16 400 cm^{-1}) and from the weak, residual emission from TiO$_2$−Ru^{II}* (635 nm, 15 800 cm^{-1}), energy transfer from Nafion,Ru(bpy)$_3^{2+}$* to TiO$_2$−Ru^{II} is favored by ∼650 cm^{-1} and expected to be rapid. This observation leads to the assumed mechanism in eq 5a with excited-state quenching dominated by the surface-adsorbed complex excited state, TiO$_2$−Ru^{II}*. It is formed by direct excitation and by "antenna" energy migration and transfer from Nafion,Ru(bpy)$_3^{2+}$*.

On the basis of the absence of emission in acidic solution, quenching by surface injection occurs with $k_q' > 10^9$ s^{-1} for TiO$_2$−Ru^{II*}. From earlier measurements in nonaqueous solvents, subpicosecond injection lifetimes have been reported for related carboxylate-bound and phosphonate-bound complexes.[18]

In the overlayer structure in eq 5a with k_q',$k_{en} \gg k_{mig}$, quenching of Ru(bpy)$_3^{2+}$* emission in Nafion is rate-limited by energy transfer migration to the interface. In this limit, the decrease in lifetime for Nafion,Ru(bpy)$_3^{2+}$* is a direct measure of $\langle\tau_{mig}\rangle$. It is related to the experimental lifetime, $\langle\tau\rangle$, and $\langle\tau_o\rangle$ by $\langle\tau\rangle^{-1} - \langle\tau_o\rangle^{-1} = \langle\tau_{mig}\rangle^{-1} = \langle k_{mig}\rangle = 1.9 \times 10^6$ s^{-1}. On the basis of the fraction of quenching that occurs compared to Nafion,Ru(bpy)$_3^{2+}$* on FTO, excitation in the overlayer results in quenching by sensitization of TiO$_2$−Ru^{II} with an efficiency of

$$\eta = \langle k_{mig}\rangle/(\langle k_{mig}\rangle + \langle k_o\rangle) = 0.49$$

Quenching is also observed in FTO|nanoTiO$_2$−Nafion/Ru(bpy)$_3^{2+}$ without the adsorbed TiO$_2$−Ru^{II} injection site. As shown in the mechanism for quenching by injection (eq 6a), in these films excited state quenching presumably occurs at sites near the TiO$_2$−Nafion interface with additional contributions from sites remote from the interface by excitation and site-to-site energy migration as in the surface derivatized films.

$$\mathrm{TiO_2|Ru(bpy)_3^{2+},Ru(bpy)_3^{2+}(naf)} \xrightarrow{h\nu} \mathrm{TiO_2|Ru(bpy)_3^{2+*},Ru(bpy)_3^{2+}(naf)} \xrightarrow{k_q} \mathrm{TiO_2(e^-)|Ru(bpy)_3^{3+},Ru(bpy)_3^{2+}(naf)} \quad (6a)$$

$$\mathrm{TiO_2|Ru(bpy)_3^{2+},Ru(bpy)_3^{2+}(naf)} \xrightarrow{h\nu} \mathrm{TiO_2|Ru(bpy)_3^{2+},Ru(bpy)_3^{2+*}(naf)} \xrightarrow{k_{mig}} \mathrm{TiO_2|Ru(bpy)_3^{2+*},Ru(bpy)_3^{2+}(naf)} \xrightarrow{k_q} \mathrm{TiO_2(e^-)|Ru(bpy)_3^{3+},Ru(bpy)_3^{2+}(naf)} \quad (6b)$$

From the lifetime data in Figure 6, for this mechanism, $\langle\tau\rangle^{-1} - \langle\tau_o\rangle^{-1} = 6.2 \times 10^5$ s^{-1}. This comparison shows that in FTO|nanoTiO$_2$−Nafion/Ru(bpy)$_3^{2+}$ the slow step is injection into the conduction band of the electrode with $\langle k_{mig}\rangle \sim 3\langle k_q\rangle$. With this value, the sensitization efficiency is $\eta \sim \langle k_q\rangle/(\langle k_o\rangle + \langle k_q\rangle) \sim 0.24$.

Assuming a quantum yield of injection of 0.24 in the working DSSC cell and given an APCE of ∼8% for FTO|nanoTiO$_2$−Nafion,Ru(bpy)$_3^{2+}$, the collection efficiency is ∼40%. For FTO|nanoTiO$_2$−[Ru(bpy)$_2$(4,4′-(PO$_3$H$_2$)$_2$bpy)]$^{2+}$/Nafion, the quantum yield for injection is assumed to be near unity based on the steady-state emission data. On the basis of this assumption, the electron collection efficiency in the DSSC is ∼8%.

For FTO|nanoTiO$_2$−[Ru(bpy)$_2$(4,4′-PO$_3$H$_2$)$_2$bpy)]$^{2+}$/Nafion-Ru(bpy)$_3^{2+}$, the injection efficiency includes contributions from both absorbers. For the sample used for the IPCE experiment, the fraction of the total surface coverage of Ru(bpy)$_3^{2+}$ was ∼34%, and Ru(bpy)$_2$(4,4′-PO$_3$H$_2$)$_2$bpy)]$^{2+}$ was ∼66%. Since the extinction coefficient for Ru(bpy)$_3^{2+}$ is ∼1.5 times greater than that for Ru(bpy)$_2$(4,4′-PO$_3$H$_2$)$_2$bpy)$^{2+}$ at the excitation wavelength (451 nm), each of the MLCT absorbers absorbs ∼50% of the incident light. Assuming that direct injection by Ru(bpy)$_3^{2+}$ is nil, the total quantum yield for injection is given by eq 7, in which α is the fraction of light absorbed by the absorber, φ is the quantum yield for injection at the surface-bound sensitizer, and η_{en} is the energy transfer efficiency from remote to surface-bound sensitizer. The total quantum yield for injection is 0.75, giving a collection efficiency of 10%.

$$\varphi_{total} = \alpha_{surface\text{-}bound}\varphi_{surface\text{-}bound} + \alpha_{remote}\varphi_{surface\text{-}bound}\eta_{en} \quad (7)$$

The ~4 times higher collection efficiency for FTO|nanoTiO_2−Nafion/$Ru(bpy)_3^{2+}$ may be due to less efficient back electron transfer following photoinjection, $TiO_2(e^-)$|Nafion,$Ru(bpy)_3^{3+}$ → TiO_2|Nafion,$Ru(bpy)_3^{2+}$, in competition with reduction of Ru(III) by I^-, 2 $TiO_2(e^-)$|Nafion,$Ru(bpy)_3^{3+}$, $I^- + I^- \rightarrow 2\ TiO_2(e^-)$|Nafion,$Ru(bpy)_3^{2+} + I_3^-$. This is presumably an additional manifestation of the exclusion of I^-/I_3^- from the local environment in the anion exchange membrane.

Conclusions

Emission spectra and lifetime comparisons reveal an "antenna" effect by $Ru(bpy)_3^{2+}$ in the composite structure FTO|nanoTiO_2-$[Ru(bpy)_2(4,4'\text{-}(PO_3H_2)_2bpy)]^{2+}$/Nafion,$Ru(bpy)_3^{2+}$. It is based on an added light absorber ion exchanged into a Nafion overlayer. Our results are only a "proof of concept" showing the feasibility of using the interior voids of nano-TiO_2 to add a function, in this case, an added antenna. Compared to FTO|nanoTiO_2−$[Ru(bpy)_2(4,4'\text{-}(PO_3H_2)_2bpy)]^{2+}$, light absorption in the antenna structure is enhanced and broadened slightly to higher energy (Figure 1). In actual applications, a more desirable configuration would involve surface attachment of a lower energy light absorber such as the dye $[Os(bpy)_2(4,4'\text{-}(PO_3H_2)_2bpy)]^{2+}$ with a higher energy absorber in the external film to create a "black" absorbing interface.

The antenna itself is only marginally efficient, with ~50% of the antenna absorbed light reaching the surface bound absorber where injection occurs. Nonetheless, our results are an important first step in utilizing the interior volumes of these nanostructured devices to add an additional function to the film interior.

Acknowledgment. Funding by the Chemical Sciences, Geosciences and Biosciences Division of the Office of Basic Energy Sciences, U.S. Department of Energy, Grant DE-FG02-06ER15788 (for time-resolved and steady state photoluminescence studies as well as XPS analysis, A.G.), and UNC EFRC: Solar Fuels and Next Generation Photovoltaics, an Energy Frontier Research Center funded by the U.S. Department of Energy, Office of Science, Office of Basic Energy Sciences under Award Number DE-SC0001011 (for sample preparation, UV-Vis, and IPCE measurements, P.G.H.), is gratefully acknowledged.

References and Notes

(1) Gratzel, M. *Inorg. Chem.* **2005**, *44*, 6841–6851.
(2) Meyer, G. J. *Inorg. Chem.* **2005**, *44*, 6852–6864.
(3) Hoertz, P. G.; Jurss, J. W.; Concepcion, J. J.; Brennaman, M. K.; Donley, C.; Meyer, T. J. To be submitted for publication.
(4) Gillaizeau-Gauthier, I.; Odobel, F.; Alebbi, M.; Argazzi, R.; Costa, E.; Bignozzi, C. A.; Qu, P.; Meyer, G. J. *Inorg. Chem.* **2001**, *40*, 6073–6079.
(5) Broomhead, J. A.; Young, C. G.; Hood, P. *Inorg. Synth.* **2007**, *21*, 127–128.
(6) Lee, S.-H.; Abrams, N. M.; Hoertz, P. G.; Barber, G. D.; Halaoui, L. I.; Mallouk, T. E. *J. Phys. Chem. B* **2008**, *112*, 14415–14421.
(7) Berberan-Santos, M. N.; Bodunov, E. N.; Valeur, B. *Chem. Phys.* **2005**, *315*, 171.
(8) Qu, P.; Meyer, G. J. *Langmuir* **2001**, *17*, 6720.
(9) Benkstein, K. D.; N; Kopidakis, N.; van de Lagemaat, J.; Frank, A. J. *J. Phys. Chem. B* **2003**, *107*, 7759–7767.
(10) Chen, P.-Y.; Meyer, T. J. *Chem. Rev.* **1998**, *98*, 1439.
(11) Thompson, D. W.; Fleming, C. N.; Myron, B. D.; Meyer, T. J. *J. Phys. Chem. B* **2007**, *111*, 6930.
(12) Jones, W. E. J.; Chen, P.; Meyer, T. J. *J. Am. Chem. Soc.* **1992**, *114*, 387.
(13) Hasselman, G. M.; Watson, D. F.; Stromberg, J. R.; Bocian, D. F.; Holten, D.; Lindsey, J. S.; Meyer, G. J. *J. Phys. Chem. B* **2006**, *110* (50), 25430–25440.
(14) Kleverlaan, C.; Alebbi, M.; Argazzi, R.; Bignozzi, C. A.; Hasselmann, G. M.; Meyer, G. J. *Inorg. Chem.* **2000**, *39*, 1342–1343.
(15) Bignozzi, C. A.; Argazzi, R.; Schoonover, J. R.; Meyer, G. J.; Scandola, F. *Sol. Energy Mater. Sol. Cells* **1995**, *38* (1−4), 187–198.
(16) Hardin, B. E.; Hoke, E. T.; Armstrong, P. B.; Yum, J.-H.; Comte, P.; Torres, T.; Frechet, J. M. J.; Nazeeruddin, Md. K.; Gratzel, M.; McGehee, M. D. *Nat. Photonics* **2009**, *3* (7), 406–411.
(17) Shankar, K.; Feng, X.; Grimes, C. A. *ACS Nano* **2009**, *3*, 788–794.
(18) She, C.; Guo, J.; Irle, S.; Morokama, K.; Mohler, D. L.; Zabri, H.; Odobel, F.; Youm, K.-T.; Liu, F.; Hupp, J. T.; Lian, T. *J. Phys. Chem. A* **2007**, *111*, 6832–6842.

JP103867J